Plasmonics (2015) 10:27–32
DOI 10.1007/s11468-014-9772-6

Fano Resonance with Ultra-High Figure of Merits Based on Plasmonic Metal-Insulator-Metal Waveguide

Kunhua Wen · Yihua Hu · Li Chen · Jinyun Zhou · Liang Lei · Zhen Guo

Received: 2 July 2014 / Accepted: 6 August 2014 / Published online: 23 August 2014

Abstract A plasmonic nano-sensor is proposed by means of Fano resonance in a metal-insulator-metal (MIM) waveguide structure, which consists of two identical slot cavities placed nearby two symmetrical grooves in a MIM bus waveguide. Due to the interaction of the broad bright mode and the narrow dark mode caused by the grooves and the side-coupled slot cavities, respectively, the transmission spectrum possesses a sharp asymmetrical profile. The spectral line shape can be manipulated by changing the length of the grooves, and the wavelength of the resonance peak has a linear relationship with the length of the slot cavity. These characteristics offer flexibility to design the device. This nano-sensor yields a sensitivity of ~903 nm/RIU and a figure of merit (FOM) of $\sim 3.1\times10^5$. Besides, dual Fano resonance peaks are also achieved by shifting the slot cavities away from the center of the grooves, resulting in a FOM as high as 4.6×10^5. The proposed structure may find important applications in the on-chip nano-sensing area.

Keywords Plasmonic nano-sensor · Fano resonance · Metal-insulator-metal waveguide

K. Wen (✉) · Y. Hu · L. Chen · J. Zhou · L. Lei
School of Physics and Optoelectronic Engineering, Guangdong University of Technology, Guangzhou 510006, Guangdong, China
e-mail: khwen@gdut.edu.cn

K. Wen
e-mail: wkh2003@gmail.com

Z. Guo
Center for Information Photonics & Communications, School of Information Science and Technology, Southwest Jiaotong University, Chengdu 610031, Sichuan, China

Z. Guo
State Key Lab of Optical Technology for Microfabrication, Chinese Academy of Science, Chengdu 610029, China

Introduction

Fano resonance, which arises from the coherent coupling and interference between a discrete state and a continuous state, possesses a distinctly asymmetric line shape [1]. Since great sensitivity and large figure of merit (FOM) can be easily achieved due to its unique characteristics, the Fano resonance has shown great potential in the sensors, switching, nonlinear, and slow light areas [2–4]. Recently, various plasmonic structures have been employed to study the Fano resonances for the reason that surface plasmon polaritons (SPPs) can overcome the diffraction limit of optical wave and provide the on-chip propagation for light [5]. The Fano resonances can be obtained through the interaction of the narrow dark modes with the broad bright modes inside those sub-wavelength structures. For example, a unit-cell structure with side-coupled detuned resonators was proposed to obtain the Fano resonances, which were also observed in a dolmen-type slab structure consisting of a radiative element and a sub-radiant element. Besides, Fano-like resonances in plasmon rulers [6], plasmonic nanoparticle clusters [7], composite cut-wire structures [8], core-shell structures [9], and other arrangements [10–13] have been investigated theoretically or experimentally. In view of the development of nano-integrated photonics, it is worth to point out that the Fano resonances are also widely studied by using the metal-insulator-metal (MIM) waveguides [14–16], which are more suitable for the highly integrated optical circuits due to their deep-sub-wavelength confinement of light [17–20].

In this paper, a MIM-waveguide-based structure is proposed to obtain the Fano resonances. A pair of slot-cavity resonators is designed close to the ends of two grooves, which symmetrically locate at both sides of a MIM bus waveguide. After transmitting into the grooves, SPPs will be coupled into the slot cavities which act as the Fabry-Perot (FP) resonators with narrowband spectral responses. Since the groove structure can also be regarded as a reflector, which provides broad

pass band, the Fano resonance will then be generated because of the interaction of two modes. The Fano resonance line shape and the peak wavelength strongly rely on the lengths of the grooves and the slot cavities, respectively. Interestingly, when the slot cavities are shifted away from the center of the grooves, dual Fano resonance peaks are achieved. The proposed sub-wavelength structure can serve as an excellent plasmonic sensor with a sensitivity of about 903 nm/RIU and a figure of merit (FOM) larger than 3.1×10^5.

Theory and Analysis

The MIM waveguide structure is shown in Fig. 1. Two grooves are symmetrically distributed in both sides of the input/output bus waveguide. Meanwhile, two identical slot cavities, which act as the FP resonators, are placed close to the ends of the grooves, respectively. As well known, the guided modes inside the MIM waveguides are significantly affected by the effective refractive index, which can be obtained from the dispersion equation [21]:

$$\varepsilon_i k_{z2} + \varepsilon_m k_{z1} \coth\left(-ik_{z1} W_{1,2}/2\right) = 0 \tag{1}$$

where $k_{z1,2}^2=\varepsilon_{i,m}k_0^2-(k_0 n_{eff})^2$ is the transverse propagation constant in the insulator or metal, $W_{1,2}$ is the insulator thickness, $k_0=2\pi/\lambda$ is the free space wave-vector, and ε_i and ε_m are the dielectric constants of the dielectric medium and the metal, respectively. Here, the metal and insulator are firstly assumed to be silver and air, respectively.

For those MIM waveguides with grooves only, broad bright modes will be achieved because of the effect analogous to the Bragg reflection [22]. Interestingly, narrow dark modes can be obtained by using the side-coupled slot-cavity structure [23, 24]. By taking advantage of the characteristics of both structures, the Fano resonance will be generated in our hybrid scheme due to the interaction between the dark mode and the bright mode. Different from the Lorentzian resonance, a distinctly asymmetrical spectral profile is achieved for the Fano resonance. Specifically, an asymmetrical transmission peak with narrow bandwidth will arise in a large wavelength range. The wavelength of the Fano resonance peak will be determined by the length of the slot cavities, expressed as

$$\lambda = \frac{2n_s L}{m-\phi/2\pi}, \quad m = 1,\ 2,\ 3,\ \cdots \tag{2}$$

where n_s is the real part of the effective index, m is the resonance order, L is the length of the slot cavity, and φ is the phase change due to the reflection at the FP facet. Note that higher-order FP resonance modes will be with smaller bandwidths, and thus the 2nd resonance mode is used here. Then the slot cavities should be with suitable length to ensure that the second resonance mode will locate at the wavelength range of the bright mode caused by the grooves. As the connection bridge of two slot cavities, the grooves provide the oscillation space for the SPPs. This could greatly affect the line shape of the transmission spectrum.

Moreover, FOM as a key factor is widely used to evaluate the performance of the Fano resonance. A relative transmittance change $dT(\lambda)/dn(\lambda)$ at fixed wavelength λ_0 will be detected for the Fano resonance, and then FOM* and FOM are defined as [25, 26]

$$\mathrm{FOM}^* = \left|\frac{dT(\lambda)/dn(\lambda)}{T(\lambda)}\right| \tag{3}$$

$$\mathrm{FOM} = \max(\mathrm{FOM}^*) \tag{4}$$

where $T(\lambda)$ is the transmittance at the specific wavelength, $dT(\lambda)/dn(\lambda)$ is the transmittance change at fixed wavelength induced by a refractive index change, and λ_0 is the corresponding wavelength where FOM is achieved. Base on Eqs. (3) and (4), it can be predicted that an ultra-low transmittance and a sharp change of the transmittance induced by the index changes are preferred for obtaining a large FOM.

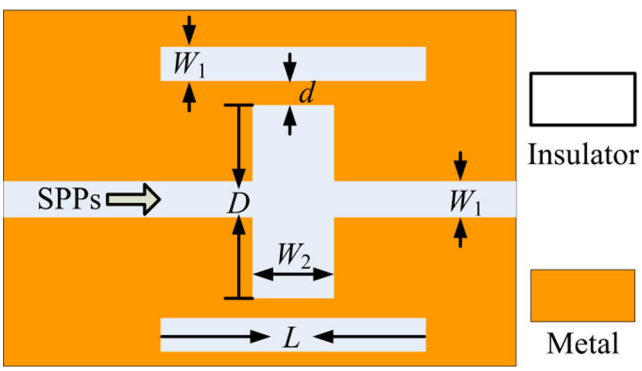

Fig. 1 Scheme diagram of the plasmonic nano-sensor-based MIM waveguides

Simulation and Discussion

In the following, FDTD method with perfect matched layer is used to investigate the performances of the proposed structure, and the grid sizes in 2D directions are set to be 5 nm×5 nm. The detailed parameters are firstly defined as the widths of the bus waveguide, and the slot cavities are the same as $W_1=50$ nm, the width and the length of the grooves are $W_2=100$nm

and D=300nm, respectively, the coupling distances from the grooves to the slot cavities are d=20nm. In addition, the experimental optical constant of silver [27] is used during the simulation.

The lengths of the slot cavities L are firstly increased from 550 to 700 nm with a step of 50 nm to investigate its influence on the Fano resonance. The simulated transmission spectra are shown in Fig. 2a, which clearly shows that asymmetrical spectral profiles are achieved for all the cases with transmittances of ~0.5. The transmittance will decrease rapidly at the right side of the sharp transmission peak, resulting in a transmission dip with ultra-low transmittance. Those bright modes are with quite small full width at half-maximums (FWHMs), i.e., 17.4, 20.0, 20.6, and 22.1 nm, respectively. This is also the desired characteristics for the sensors. Besides, the peak wavelengths and the dip wavelengths are 863.2 and 891.0 nm, or 931.4 and 955.1 nm, or 999.7 and 1020.1 nm, or 1066.8 and 1086.7 nm when the lengths of the slot cavities L are 550, 600, 650, or 700 nm, respectively. Fig. 2b gives a more detailed analysis on the wavelength variations with respect to the lengths of the slot cavities, which are increased from 550 to 700 nm with a step of 10 nm. In this case, the growth step of the peak wavelength or the dip wavelength is uniform

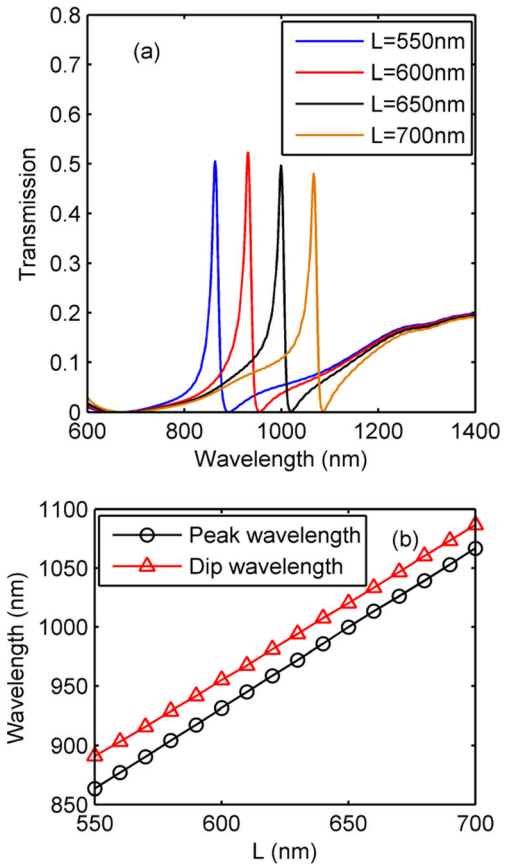

Fig. 2 **a** Transmission spectra with different lengths of slot cavities and **b** the peak-wavelength and dip-wavelength variations with the lengths of slot cavities

as about 13.6 or 13.0 nm. Obviously, the wavelength has a linear relationship with L, and the results agree well with the theoretical analysis of Eq. (2). Then, one can easily manipulate the wavelength by adjusting the lengths of the slot cavities.

Figure 3 shows the magnetic field intensity distributions of SPPs at the peak wavelengths and the dip wavelengths that correspond to the results in Fig. 2a. Most of the SPPs at the peak wavelengths can pass through the bus waveguide (Figs. 3a, c, e, g) while those at the dip wavelengths are completely stopped in the waveguide (Figs. 3b, d, f, h). These straightforward results provide the SPP power flows in our proposed structure in detail.

Besides, the results in Fig. 2a indicate that the wavelength shifts from the peaks (corresponding to an "on" state) to the valleys (corresponding to an "off" state) are about 27.8, 23.7, 20.4, and 19.9 nm, respectively. Such a short wavelength change can provide a high sensitivity of spectrum response to the index variations of nearby or surrounding medium for the structure. Therefore, the insulator with different refractive index n is employed to investigate the spectral response. The lengths of the slot cavities are fixed as 600 nm, and other parameters are the same as those for Fig. 2a. The transmission spectra are show in Fig. 4, which indicates that the transmission peaks with transmittances of about 0.52 are at 931.4, 940.5, 949.1, 958.6, and 967.5 nm when n=1.00, 1.01, 1.02, 1.03, and 1.04, respectively. The resonance wavelength has a redshift when increasing the refractive index and almost increases linearly. Then the sensitivity is derived as about 903 nm/RIU.

In the following, the length of the groove D is also studied to investigate the transmission spectrum. The lengths of the slot cavities are fixed as 600 nm while other parameters keep

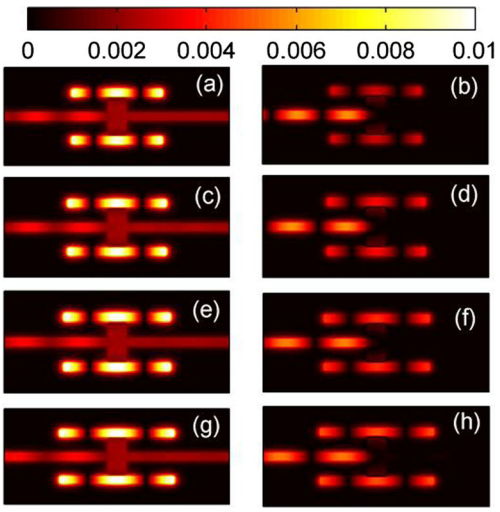

Fig. 3 Magnetic field intensity distributions of SPPs at the peak wavelengths and the dip wavelengths that correspond to the results in Fig. 2a. The lengths of the slot cavities are 550 nm in **a** and **b**, 600 nm in **c** and **d**, 650 nm in **e** and **f**, and 700 nm in **g** and **h**

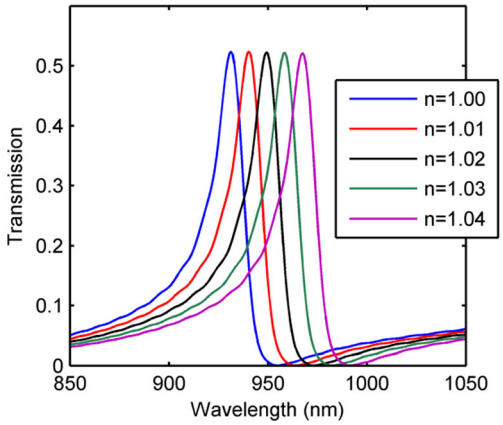

Fig. 4 Transmission spectra based on different refractive indices of insulator

the same as above. By defining D as 320, 400, and 480 nm, we obtain the transmission spectra in Fig. 5a–c, respectively. The asymmetrical profile of the transmission spectrum presents an obvious transformation by increasing D. Specifically, the dip arises at the right side of the peak in Fig. 5a, and then the transmittance increases rapidly with the wavelength. However, the transmission spectrum shows an inverse line shape in Fig. 5c, where the transmittance will decrease firstly with wavelength and the dip arises in the left side of the peak. A transition state is presented in Fig. 5b, where the dip at the right side of the peak will disappear gradually and another one will emerge at the left side. In this case, narrow Lorentzian-like line-shape transmission windows are approximately constructed. Moreover, the magnetic field distributions are provided at the wavelengths of 932.2 and 957.7 nm in Fig. 5a; 849.9, 937.2, and 995.9 nm in Fig. 5b; and 908.8, and 941.4 nm in Fig. 5c, respectively. They clearly illustrate the propagation details of SPPs at the dip wavelengths and the peak wavelengths. To better evaluate the performance of the plasmonic sensor, the FOM is studied in detail. Based on Eqs. (3) and (4), FOM* corresponding to the case in Fig. 5

Fig. 5 Transmission spectra with different lengths of grooves

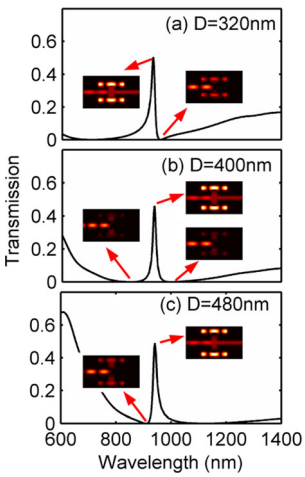

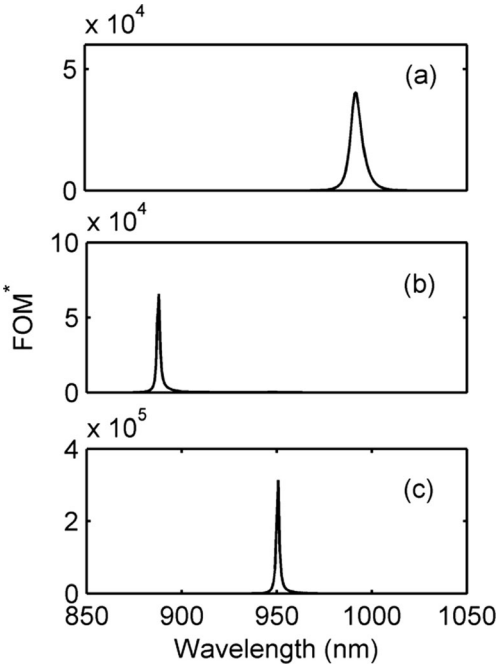

Fig. 6 The calculated FOM* corresponding to Fig. 5

(i.e., D=320, 400, and 480 nm) is shown in Fig. 6 by changing the refractive index of the insulator from 1.00 to 1.05. The values of FOM are 4.0×10^4, 6.6×10^4, and 3.1×10^5 in Figs. 6a–c, respectively. These FOM values are significantly greater than that in the previous reports [14, 25, 26].

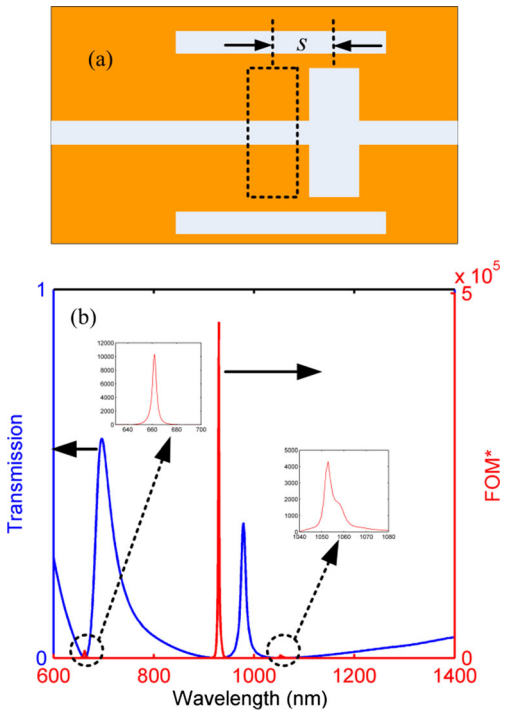

Fig. 7 **a** Structure with asymmetry of slot cavities, **b** transmission spectrum with dual Fano resonance peaks (*blue line*), and the calculated FOM* (*red line*)

According to the outstanding properties, it is demonstrated that the proposed structure can work as a sensor well.

Furthermore, one interesting phenomenon is also found and studied. When the cavities are shifted away from the center of the grooves (shown in Fig. 7a), two Fano resonance peaks arise. By defining the shift s=100 nm, D=300 nm, L=600 nm, and d=15 nm, we obtain the transmission spectrum in Fig. 7b based on FDTD method. The transmittances or the FWHMs for two Fano resonance peaks are 0.595 and 0.367 or 41.8 and 11.7 nm at the wavelengths of about 696.4 and 978.3 nm, respectively. The dual-channel Fano resonance effect is mainly caused by the symmetry breaking of the structure. When SPPs are captured into the slot cavities, they will be separated into the left side or the right side of the cavities. Then, additional peaks will arise due to the resonance effect contributed from two different optical paths. Besides, FOM* is also provided to investigate the performance of the sensor by using the refractive index n=1.05. An ultra-high FOM of 4.6×10^5 is available at 929.7 nm (i.e., the position of the original Fano resonance dip in Fig. 7b). There are also two dips with high FOM of 1.0×10^4 and 4.3×10^3 at the wavelengths of 661.7 and 1052.9 nm, respectively, as shown in the inset.

Conclusion

In summary, Fano resonance has been demonstrated in our proposed MIM waveguide structure, which consisted of a pair of symmetrical grooves and slot cavities. A sharp transmission peak was achieved at a broad wavelength range. The asymmetrical line shape and the resonance wavelength can be manipulated by changing the lengths of the grooves and the slot cavities, respectively. The sensitivity and the FOM were as high as 903 nm/RIU and 3.1×10^5. Interestingly, dual Fano resonance peaks have also been obtained by shifting the slot cavities away from the center of the grooves. In this case, the highest FOM was 4.6×10^5 at the wavelength 929.7 nm. Therefore, the structure can find widely applications in the plasmonic nano-sensing area.

Acknowledgements This work is supported by the China Postdoctoral Science Foundation (No. 2014 M552173), the Open Research Fund of State Key Lab of Optical Technologies for Micro-Engineering and Nano-Fabrication of China, and the Research Fund of Guangdong University of Technology (No. 13ZK0387).

References

1. Luk'yanchuk B, Zheludev N, Maier S, Halas N, Nordlander P, Giessen H, Chong C (2010) The Fano resonance in plasmonic nanostructures and metamaterials. Nat Mater 9(9):707–715
2. Miroshnichenko E, Flach S, Kivshar YS (2010) Fano resonances in nanoscale structures. Rev Mod Phys 82(3):2257–2298
3. Verellen N, Sonnefraud Y, Sobhani H, Hao F, Moshchalkov VV, Van Dorpe P, Nordlander P, Maier SA (2009) Fano resonances in individual coherent plasmonic nanocavities. Nano Lett 9(9):1663–1667
4. Chen JJ, Li Z, Zhang X, Xiao JH, Gong QH (2013) Submicron bidirectional all-optical plasmonic switches. Sci Rep 3:1451
5. Barnes WL, Dereux A, Ebbesen TW (2003) Surface plasmon subwavelength optics. Nature 424(6950):824–830
6. Liu N, Hentschel M, Weiss T, Alivisatos AP, Giessen H (2011) Three-dimensional plasmon rulers. Science 332(6036):1407–1410
7. Fan JA, Wu C, Bao K, Bao J, Bardhan R, Halas NJ, Manoharan VN, Nordlander P, Shvets G, Capasso F (2010) Self-assembled plasmonic nanoparticle clusters. Science 328(5982):1135–1138
8. Artar A, Yanik AA, Altug H (2011) Directional double Fano resonances in plasmonic hetero-oligomers. Nano Lett 11(9):3694–3700
9. Hu Y, Noelck SJ, Drezek RA (2010) Symmetry breaking in gold-silica-gold multilayer nanoshells. ACS Nano 4(3):1521–1528
10. Wang JQ, Fan CZ, He JN, Ding P, Liang EJ, Xue QZ (2013) Double Fano resonances due to interplay of electric and magnetic plasmon modes in planar plasmonic structure with high sensing sensitivity. Opt Express 21(2):2236–2244
11. Zhang ZS, Yang ZJ, Li JB, Hao ZH, Wang QQ (2011) Plasmonic interferences in two-dimensional stacked double-disk array. Appl Phys Lett 98(17):173111
12. Fang ZY, Cai J, Yan Z, Nordlander P, Halas NJ, Zhu X (2011) Removing a wedge from a metallic nanodisk reveals a Fano resonance. Nano Lett 11(10):4475–4479
13. Zhang S, Bao K, Halas NJ, Xu H, Nordlander P (2011) Substrate-induced Fano resonances of a plasmonic nanocube: a route to increased-sensitivity localized surface plasmon resonance sensors revealed. Nano Lett 11(4):1657–1663
14. Chen J, Li Z, Zou Y, Deng Z, Xiao J, Gong Q (2013) Coupled-resonator-induced fano resonances for plasmonic sensing with ultra-high figure of merits. Plasmonics 8(4):1627–1631
15. Piao X, Yu S, Koo S, Lee K, Park N (2011) Fano-type spectral asymmetry and its control for plasmonic metal-insulator-metal stub structures. Opt Express 19(11):10907–10912
16. Qi J, Chen Z, Chen J, Li Y, Qiang W, Xu J, Sun Q (2014) Independently tunable double Fano resonances in asymmetric MIM waveguide structure. Opt Express 22(12):14688–14695
17. Wen KH, Yan LS, Pan W, Luo B, Guo Z, Guo YH, Luo XG (2014) Electromagnetically induced transparency-like transmission in a compact side-coupled T-shaped resonator. J Lightwave Technol 32(9):1701–1707
18. Wen KH, Yan LS, Hu YH, Chen L, Lei L (2014) A plasmonic wavelength-selected intersection structure. Plasmonics 9(3):685–690
19. Song G, Yu L, Wu C, Duan G, Wang L, Xiao J (2013) Polarization splitter with optical bistability in metal gap waveguide nanocavities. Plasmonics 8(2):943–947
20. Liu Y, Zhou F, Yao B, Cao J, Mao Q (2013) High-extinction-ratio and low-insertion-loss plasmonic filter with coherent coupled nano-cavity array in a MIM waveguide. Plasmonics 8(2):1035–1041
21. Dionne JA, Sweatlock LA, Atwater HA (2006) Plasmon slot waveguides: towards chip-scale propagation with subwavelength-scale localization. Phys Rev B 73:035407

22. Lin XS, Huang XG (2008) Tooth-shaped plasmonic waveguide filters with nanometeric sizes. Opt Lett 33(23):2874–2876
23. Ma FS, Lee C (2013) Optical nanofilters based on meta-atom side-coupled plasmonics metal-insulator-metal waveguides. J Lightwave Technol 31(17):2876–2880
24. Wen KH, Yan LS, Pan W, Luo B, Guo Z, Guo YH, Luo XG (2013) Design of plasmonic comb-like filters using loop-based resonators. Plasmonics 8(2):1017–1022
25. Becker J, Trügler A, Jakab A, Hohenester U, Sönnichsen C (2010) The optimal aspect ratio of gold nanorods for plasmonic bio-sensing. Plasmonics 5(2):161–167
26. Lu H, Liu X, Mao D, Wang G (2012) Plasmonic nanosensor based on Fano resonance in waveguide-coupled resonators. Opt Lett 37(18): 3780–3782
27. Johnson PB, Christy RW (1972) Optical constants of the noble metals. Phys Rev B 6:4370–4379